Performance of DS-CDMA Protocols in Wireless LANs

M. Parikh, P. Sharma, R. Garg, K. Chandra and C. Thompson

Center for Advanced Computation and Telecommunications
University of Massachusetts Lowell
Lowell, MA. 01854

ABSTRACT

The performance of direct-sequence code-division multiple access (DS-CDMA) systems in indoor wireless channels is presented. TCP traffic, channel noise and signal characteristics are measured using commercial products that implement the IEEE 802.11b DS-CDMA standard. The measured throughputs for a low density mobile network are typically around 4.2 Mbps when one of the two end-systems is on the wired segment. Multipath interference is shown to contribute to significant degradation in TCP performance. Packet loss rates ranging from 0.02 to 0.2 percent are observed in line-of-sight conditions. The BER performance of DS-CDMA is estimated using an image source based channel model of the rectangular room to compute the spatial variation of the channel impulse response. These impulse responses provide a quantitative measure of the system performance and provide estimates of signal power levels required for supporting high data rates in channels influenced by multipath interference.

Keywords: multipath, channel impulse response, image sources, DS-CDMA, TCP, IEEE 802.11b

1. INTRODUCTION

The IEEE 802.11 standards[1,2] for wireless local area networks (WLAN) have enabled a cost-effective solution for tetherless connectivity in indoor environments. Using off-the-shelf wireless network interface cards and base stations that adopt this standard, mobile systems can be readily integrated within a wired network. The 802.11 standards define the medium access control (MAC) and physical (PHY) layer signaling and service protocols for radio transmission in the unlicensed 2.4-2.485 Ghz frequency band. The IEEE 802-11b standard is a recent high-rate extension that supports rates of 5.5 and 11 Mbps in addition to the earlier 1 and 2 Mbps bit rates. The 1 Mbps rate is generated using differential binary phase shift keying (BPSK) and direct-sequence spread spectrum (DSSS) modulation with a 11 chip Barker code. The higher rates use quadrature phase shift keying as the modulation scheme. The 11 and 5.5 Mbps rates are achieved through the use of complementary code keying to spread the transmission bandwidth. At the MAC level, the carrier-sense, multiple access collision avoidance (CSMA/CA) protocol is used to resolve contention on a common channel. Unlike collision detection in the wired Ethernet protocol, collision avoidance is implemented to optimize wireless channel usage.

The performance of 802.11b products has been presented[3–6] in several studies. Kamerman and Aben[3] investigate the effect of protocol overhead on throughput performance. TCP throughput was found to be about 47% at 11 Mbps data transfer rates. This reduction was attributed to the overhead generated by the TCP, MAC and PHY layers and due to the protocol specified wait times between transmissions. The collisions that typically ranged from $1-3\%$ also contribute to the overhead. In[5] TCP throughput was found to be on the order of 5 Mbps in line of sight (LOS) conditions and in the range of $0.5-4.5$ Mbps in non-LOS positions of the receiver. The long idle times between TCP server transmissions were attributed to be the dominant cause of performance degradation.

At the specified data rates, bit durations are on the order of tens to hundreds of nanoseconds which are comparable to the mean excess delay and delay spread values[7] observed in indoor channels. Experimental studies in indoor environments are presented in[8–10] for the 2.4 Ghz frequency. Janssen et. al[8] showed that the rms delay spread ranged from $10-70$ nsecs as the transmitter receiver distance increased and it was particularly high when measurements were made in a hallway in close proximity to the walls. Zepernick and Wysocki[9] measured

channel impulse responses in a rectangular room filled with equipment and found the mean excess delay and rms delay spread ranged from $43-57$ and $22-31$ nsecs respectively. In general, the multipath delay spread value will be a function of the room dimensions, its contents, receiver location and the reflection coefficient of the walls.

Spread-spectrum modulation schemes are expected to be robust against multipath interference. The spreading increases the transmitted signal bandwidth and typically results in it being wider than the channel coherence bandwidth. This feature is expected to mitigate frequency selective fading and intersymbol interference effects of the channel. Turin[11] presents an analysis of the performance of spread-spectrum systems in multipath and discusses the design of optimal multipath receivers that accentuate the transmitted signal based on statistics of multipath delays, amplitudes and phases. The design of a receiver that combats multipath depends on the duration of the multipath signal relative to symbol duration. For multipath delay spreads that are well within a symbol interval , when the multipath is resolvable, a receiver can take advantage of multipath diversity to obtain a more reliable estimate of the transmitted symbol. When the delay spread is larger than a symbol duration, the process of intersymbol interference must be handled using equalizers. The time interval between dominant multipath signals determines the required sampling rate at the receiver and also the bandwidth of the transmission signal.

In this paper, the TCP performance of IEEE 802.11b protocols is examined and correlated to the expected multipath delays in an indoor channel. In Section 2 measurements of TCP traffic and channel characteristics are presented. Section 3 describes an indoor channel model that provides estimates of the channel impulse response at the receiver positions. Section 4 evaluates the performance of DS-CDMA in multipath channels. Section 5 concludes the paper.

2. TCP PERFORMANCE ON WIRELESS LANS

2.1. Experimental Setup

The performance of 802.11b protocol was measured using commercially available base stations and wireless cards. The Apple *Airport* base station was used as the AP to the wired network. The mobile terminals consisted of Windows based PCs and Linux based systems equipped with the Lucent *Orinoco* network interface card and MAC *Ibooks* that were wireless enabled with the *Airport* card. The base station was connected to the wired segment of the Ethernet through a 100 Mbps hub.

The measurements were carried out in the CACT laboratory and office space at the University of Massachusetts Lowell. The room has width, length and height of approximately (55, 34, 9) feet respectively. A schematic of the space and locations of the AP and mobile receivers is shown in Fig. 1. The room includes cubicle spaces, computing equipment and a conference area. One side of the room, shown with a thick line is a brick wall. The other sides are made of plaster board. The ceiling is covered with Celotex tiles. Location A at a radius of 13 feet from the AP corresponds to a direct LOS position. Location B at a radius of 24 feet is partly obstructed from the AP by a row of steel cabinets marked in the figure by a solid color. Location C near the origin at a radius of 37.6 feet from the source is in a corner of the room and in front of a glass door framed with metal. The shaded regions represent metallic pillars in the room. The height of the mobile at all locations is maintained at 2.5 feet. The AP is mounted as shown on the brick wall at a height of 6.5 feet. The performance of the infrastructure mode of network connectivity is examined in a single user mode, where the server resides on the wired segment serving a single mobile client at a time. The server and the MS communicate through the AP.

For each measurement, a TCP flow was generated between the server and a client, transferring approximately 500 Mbytes of data. The server was configured to transmit the packets at a maximum achievable rate. The MTU at the host Ethernet interface was set to 1500 bytes. TCP packet header traces were captured at the server, the AP and the client using the *tcpdump* utility. The measurement traces include the timestamp at microsecond resolution, the source and destination host addresses, TCP sequence (SEQ) and acknowledgement (ACK) numbers, packet size and receiver window size. All networked system clocks involved in the measurements

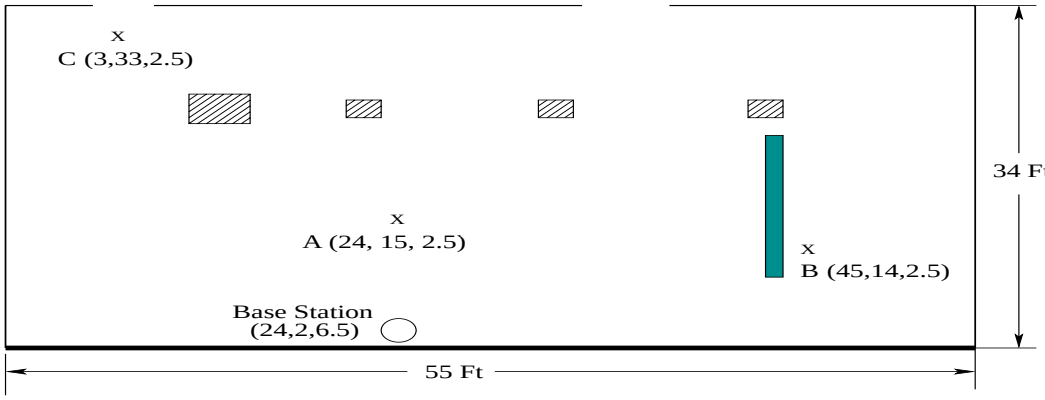

Figure 1. Schematic of measurement environment. (X denotes measurement locations)

were synchronized using the network time protocol. During the measurement, a channel sensing utility provided by the *Lucent Orinoco* network interface card was run on the mobile system to record the local and remote noise and signal levels and corresponding signal to noise ratio (SNR) measurements on the wireless link. These measurements provide an estimate of the degree of the channel interference and fading during the measurement period. At each of the three positions A, B, C in Fig. 1, the channel noise and signal levels and TCP packet headers were collected for six sets of measurements. The TCP throughput averaged over all measurement ensembles was fairly stationary around 4.2 Mbps. However the TCP retransmission and packet collision statistics were observed to be highly location dependent.

2.2. Channel Noise and Signal Measurements

The channel noise measurements are obtained during the protocol specified idle time interval between transmission of a data frame and receipt of an ACK at the physical layer. The ensemble averaged probability mass functions of the channel noise power at the measured resolution of one *dbm* are depicted in Figs. 2. The magnitude and rate of variation in noise levels in time influences the performance of the wireless link. In response to changes in channel noise levels, the protocol adapts both the transmitted power level and the transmission rate. A comparison of local (MS) and remote (AP) noise power levels N_L and N_R showed that the remote noise power was typically $7-10$ dBm lower than that at the mobile. The distribution of remote noise power shown in Fig. 2(b) is approximately stationary for all the measurement locations. The distinct bimodal distribution of local noise power in Fig. 2(a) was observed at all locations indicating that the channel may be influenced by other devices operating in the ISM frequency band causing a switching effect between two dominant noise power levels. Location specific features of the noise power can be identified at C. Here, the bi-modal characteristic broadens and suggests the presence of additional noise effects not evident at A and B.

The operating signal power levels at the AP and MS were also analyzed for the mean trend and distribution with position. The signal level distributions are depicted in Fig. 3. To compensate for the difference in local and remote noise power, the remote signal levels are typically $5-8$ dbm lower than the signal power levels at the mobile. Fig. 3 shows distinct shifts in the mean value of the signal power with position. The path loss increases as the receiver moves from position A to C. Another site dependent characteristic is the higher variance in signal power at location B and relatively lower variance about the mean for location C. This feature may indicate that the power control feature is highly activated at B. Therefore channel fading effects may be more dominant at B than at C. In contrast, given the higher variance in noise characteristics at C, the relatively narrow signal variations at C suggests that power control may be ineffective and channel is influenced by other effects not captured by the ambient noise variations. From the noise and signal power measurements, the operating SNR at the AP and mobile can be determined. The SNR variation at the mobile typically ranges from $20-40$ dB at locations B and C, whereas closer to the AP at location A it is found to range from $35-55$ dB. An estimate of the path loss exponent with distance was determined using the local signal level as a reference. For this parameter, the measurements were conducted from a radius of $5-65$ feet from the AP and at various angles.

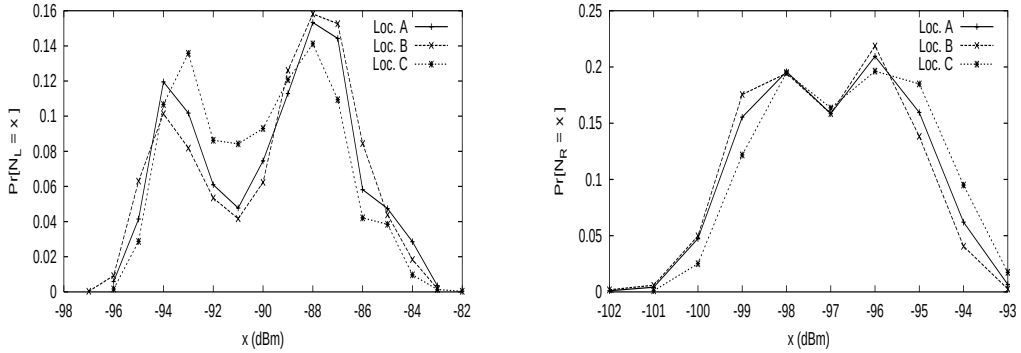

(a) (b)

Figure 2. Local (a) and Remote (b) noise power distribution.

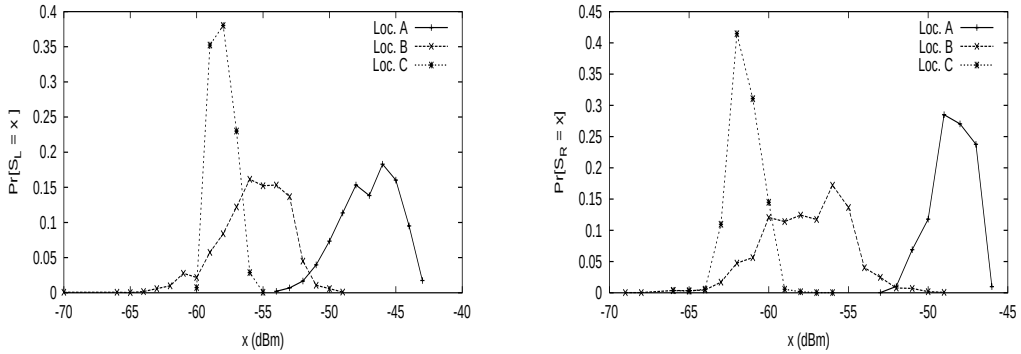

(a) (b)

Figure 3. Local (a) and Remote (b) signal power distribution.

The average value and its dispersion are shown in Fig. 4. The vertical axis is the average SNR value in decibels and the horizontal axis is the logarithm of radial distance from the AP to the MS spanning the entire room. The SNR values are averaged over different locations at the same radial distance. The values from the experiments are marked with "x" and the error bars depict the range of one standard deviation about the average value. A maximum SNR variation of $\pm 10dB$ is observed at approximately the center of the room. The dotted line is the linear model obtained from a mean-square error regression fit through the measurements. The SNR variation can be represented as $1/d^n$, where the path loss exponent $n = 2.85$. The decay rate falls within the expected range[7] of 2.4 to 3.0 for an office environment.

2.3. TCP Performance

Position dependent effects of the DS-CDMA protocol and system performance are more evident in the TCP traffic and control parameters. TCP transmits data segments using sequence numbers in byte increments to identify the position of the data stream in each packet. The receiver acknowledges each packet with an ACK number that is the sequence number it next expects to receive. The source maintains a retransmission timeout value for each TCP segment. The timeout is adaptively updated with the round-trip-times measured between transmission of a TCP segment and receipt of its ACK. If the ACK's are not received during this time, the congestion window size is reduced and the packet is retransmitted. In some situations, the receiver may send duplicate ACKs when packets are received out of order. In this case, the source waits until at least three duplicate ACKs are received before a fast retransmit is enabled without waiting for timeout to expire.

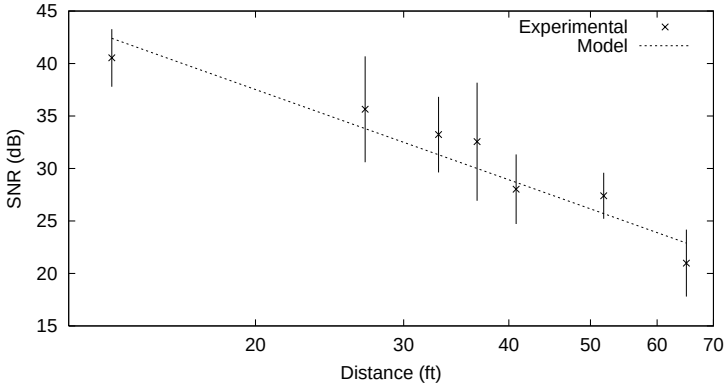

Figure 4. Variation of mean SNR with range

TCP performance in WLAN environment is negatively influenced by the high uncertainty in the expected return times for ACKs. This feature results from the wireless channel interference and fading which is typically non-stationary in indoor environments. The uncertainty is also enhanced by the rate adaptation enforced by the protocol at the MAC and PHY layers. The wireless channels can therefore experience higher packet losses than the wired medium. Packet losses may be identified by retransmission events in the TCP server log. In the protocol under study, there is a provision for the AP to also retransmit packets that are considered lost due to collision in the wireless segment. As a result, the analysis of the packet header traces collected at the mobile, reveal several instances of a unique sequence number. When the number of such occurrences are not matched by retransmission events in the TCP server data, the packet can be concluded as having experienced a collision. Collision is detected by the AP typically before the source TCP timeout period occurs. In situations where collisions occur and cause excessive delays due to the backoff in transmission time, the timeout period can exceed at the receiver and cause TCP server to retransmit.

In this study, the error packets are classified as either retransmitted packets or collision packets. Retransmitted packets are identified by their multiple occurrences in the server log. Multiply occurring packets at the receiver log that have not been classified as retransmits belong to the collision packet set. The TCP throughput and the maximum and minimum percentage of packet retransmissions and collisions are shown in Table 1.

Location	Throughput	Retransmissions (%)		Collisions (%)	
	Avg.	Max	Min	Max	Min
A	4.093	0.016	0.002	0.016	0.002
B	4.18	0.130	0.059	0.067	0.033
C	4.18	0.235	0.200	0.097	0.06

Table 1. Comparison of TCP throughput, Retransmissions and Collisions

The least number of retransmissions and collisions were observed at the LOS location A. The number of collisions increased marginally from location B to C but a higher rate of packet retransmissions was observed at C. From these observations, the channel at locations A, B and C may be characterized as good, moderate and bad channels.

The packet collisions observed in the experiment may be attributed to the collisions between TCP data forwarded from the AP and the ACK transmission by the mobile in the reverse direction. In[4] the effect of channel collisions between forward TCP data and reverse acks is shown to increase error rate. The MTU or frame size has also been found to affect the collision probability. In[12] analysis of WaveLAN showed a frame error rate of 1.55% with clustered losses when 1400 byte frames were transmitted over 85 ft distance. Reducing frame size to 300 decreased frame error rate by half albeit at the expense of higher framing overhead.

In Figs. 5 the TCP sequence number is plotted as a function of the timestamps at the receiver. The traces span the the entire measurement duration. The retransmitted packets are marked by short impulses with symbols. The collisions are identified by the longer impulses in the figure. The TCP performance data indicates not only a progressive deterioration in performance from A to C, but also suggests that increased packet retransmits at C may arise from excessive delays during transmission backoffs when increased channel noise levels fail to signal a clear channel.

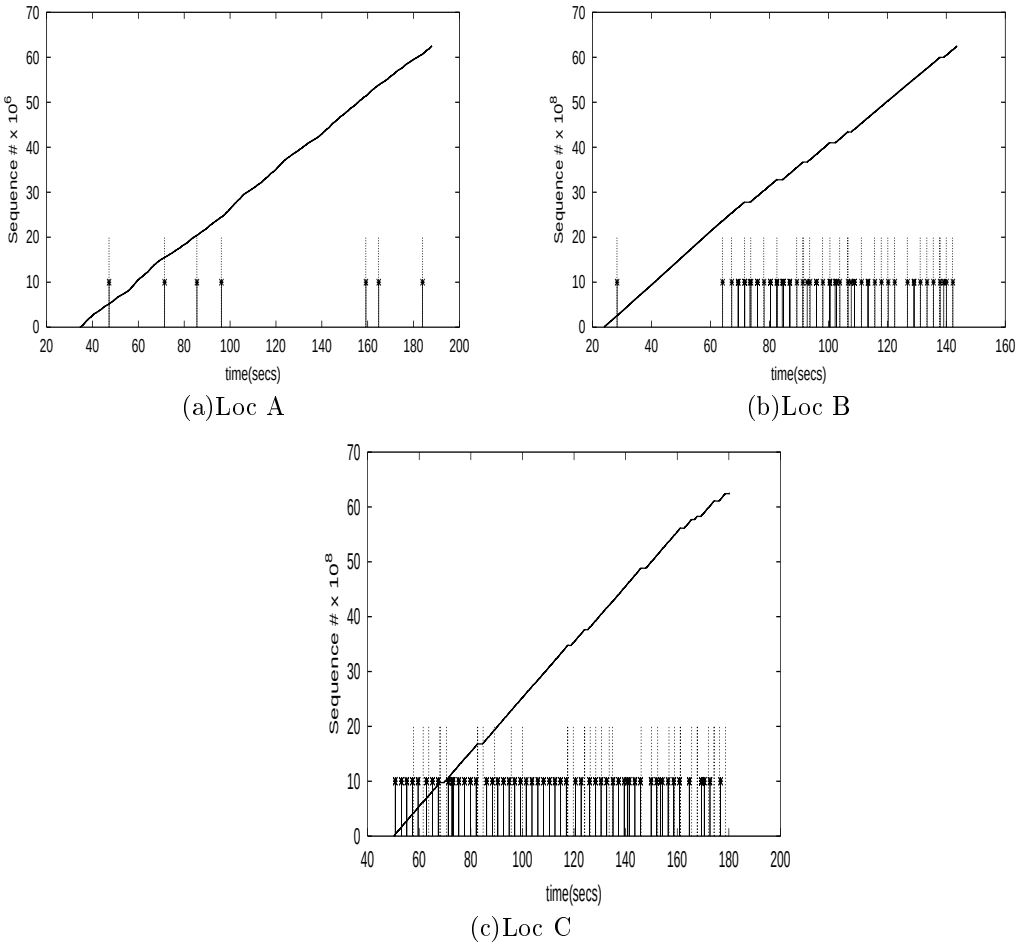

(a)Loc A (b)Loc B

(c)Loc C

Figure 5. TCP sender sequence numbers, retransmissions and collisions with time

Finally, the impact of channel and protocol induced interference on TCP traffic characteristics is examined. The sequence of packet interarrival times t_{iat} at both the AP and the mobile, the time intervals between retransmissions t_{re} and the time between collisions t_{col} are analyzed with respect to their average values, variance and marginal distribution functions. Table 2 records the time averaged values of t_{iat} in seconds, taken from six measurement sequences at the AP and mobile and t_{re} and t_{col} in milliseconds. The mean interarrival time is fairly constant with location and therefore the throughput is constant. The variance of the packet interarrival times however increase substantially from A to C.

The complementary distribution function $Pr(t_{iat} > \tau)$ is plotted against τ in Fig. 6 (a) for the AP and in (b) for the MS for the three locations. The long tails for B and C and the corresponding higher probability of their occurrence for C provides a measure of comparison of channel qualities at B and C. It indicates that the frequency of retransmissions is higher at C than at A. This is further verified by the distribution functions

Location	t_{iat}: Access Point		t_{iat}: Mobile		t_{re}		t_{col}	
	μ	σ^2	μ	σ^2	μ	σ^2	μ	σ^2
A	2.98 ms	0.009 ms	2.98 ms	0.003 ms	35.35 s	503.39 s	35.35 s	503.68 s
B	2.68 ms	0.16 ms	2.68 ms	0.146 ms	2.27 s	12.35 s	4.36 s	3.4 s
C	2.92 ms	3.84 ms	2.93 ms	3.59 ms	1.31 s	1.13 s	25.2 s	8.8 s

Table 2. Comparison of Interarrival Time Statistics

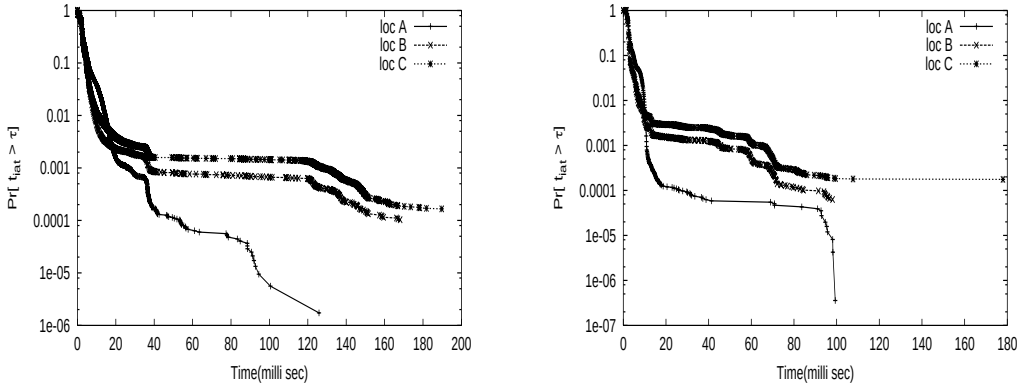

Figure 6. Complementary distribution function for Packet Interarrival Time (a) At AP (b) At MS

for the time between retransmissions and collisions shown in Fig. 7 (a-b). The smaller magnitudes of the mean value and variance for C suggest it to be a relatively predictable phenomenon in comparison to the statistics measured for location B. On the other hand, the collision rate statistics are comparable for both locations.

Several hypotheses have been put forth in this section based on the observation of the TCP traffic characteristics and channel signal and noise features. In the next section, a channel model is described that provides estimates of the channel impulse response and its multipath features for the measurement configuration considered in this section. Although the model predicts the channel response for an empty room, it still provides a baseline and conservative characterization of the position dependent response.

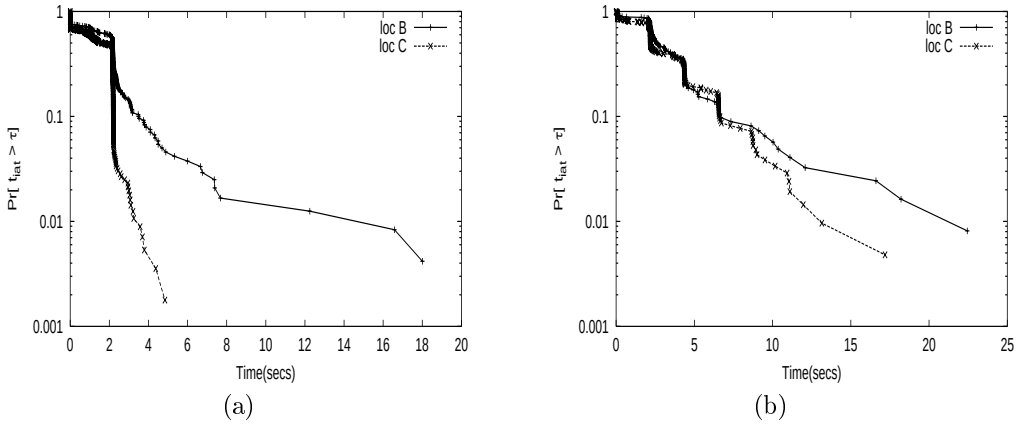

Figure 7. Complementary distribution function for Interarrival Time between (a) Retransmissions and (b) Collisions

3. INDOOR CHANNEL MODEL

The multipath characteristics of an empty rectangular enclosure are determined using the method of images. In the image method,[13–15] the walls of the enclosure are replaced by point sources of varying strength and location. The component amplitude f_i of the i^{th} image is chosen such that the transverse electric and magnetic fields are continuous across the reflecting boundary. The rectangular room is represented by the dimension L_i for the $i = 1, 2, 3$ coordinate directions. The transmitter is an electric dipole placed at location vector $\underline{r}^s$. The orientation of the dipole is given by the unit vector $\underline{u}$. The relative dielectric constant of each of the six walls is considered homogeneous in space and is given by the parameter ϵ. The receiver or observer location is denoted as $\underline{r}^o$. The positions of the image sources are $\underline{r}^i(\underline{K})$, where $\underline{K} = (K_1, K_2, K_3)$, K_j being the image count along the j^{th} axis.

The image locations are given by,

$$r_j{}^i(K_j) \;=\; 2\left[\frac{K_j}{2}\right]_{ceil} L_j \;+\; (-1)^{K_j} r_j{}^s \tag{1}$$

for $K_j : (-\infty, \infty)$. The image position $\underline{r}^i(\underline{K})$ at index $\underline{K} \;=\; (0,0,0)$ corresponds to the source position $\underline{r}^s$.

The evolution of the electromagnetic wave in space and time can be described in terms of the Hertz vector $\underline{\Pi}$.

$$\Pi_j(\underline{r}^o, \underline{r}^s, t) \;=\; \sum_{\underline{K}} \frac{f_j\left(\frac{ct}{X_{\underline{K}}} - 1, \underline{K}\right)}{X_{\underline{K}}} \tag{2}$$

where c is the speed of light and $X_{\underline{K}} = |\underline{r}^o - \underline{r}^i(\underline{K})|$.

The Fourier transform of the j^{th} component of the Hertz vector due to the $\underline{K}$ image is given in terms of the reflected components as,

$$F_j(\omega, \underline{K}) = R_j^{K_1} R_j^{K_2} R_j^{K_3} \tag{3}$$

where $R_j^{K_i} \quad j = 1, 2, 3$ represent the components of the vector Fourier amplitudes of the reflected waves resulting from the image sources along K_i direction. The iterative computation of these components is described[16] in previous work by Sharma et. al.

Inverting the transform yields the causal signal

$$f_j(t\frac{c}{X_{\underline{K}}}, \underline{K}) = \int_0^\infty F_j(\omega, \underline{K}) e^{-i\omega t \frac{c}{X_{\underline{K}}}} d\omega \tag{4}$$

which when substituted in Eq. 2 yields the Hertzian potential.

The denominator $X_{\underline{K}}$ in Eq. 2 reflects the decay in amplitude with distance that results from the spherical spread of the field generated by the image source. Ideally one would like the signal at the observation point to be simply a time-shifted version of the input signal. However, wall reflections serve to distort the signal by superposing both weighted and time shifted versions of the original signal.

A discrete-time representation of the function in Eq. 2 can be obtained by sampling the waveform in time at intervals of T_s, $t = nT_s$. This corresponds to a spatial sampling at intervals of cT_s. Hence the nondimensional distance between the source and the $\underline{K}$ image is $M_{\underline{K}} = X_{\underline{K}}/(cT_s)$ Relating the Hertzian to the vector electric field $\underline{E}$ [17] , the j^{th} component of the electric field E_j for discrete time and space is

$$E_j(\underline{r}^o, \underline{r}^s, n) = \sum_{p=1}^{3} \sum_{\underline{K}} \frac{\cos(\beta_j)\cos(\beta_p) - \delta_{jp}}{M_{\underline{K}}} \left[\ddot{f}_p(n/M_{\underline{K}} - 1, \underline{K})i + \frac{\dot{f}_p(n/M_{\underline{K}} - 1, \underline{K})}{M_{\underline{K}}} + (3 - \delta_{jp})\frac{f_p(n/M_{\underline{K}} - 1, \underline{K})}{M_{\underline{K}}^2}\right] \tag{5}$$

where $\cos(\beta_j) = (r_j{}^o - r_j{}^i(\underline{K}))/X_{\underline{K}}$, $\dot{f}$ and $\ddot{f}$ correspond to the first and second derivatives with respect to the function's argument.

The aforementioned model will be applied to estimate the multipath characteristics in a room comparable in size and shape to that in which the measurements were carried out. The room dimensions are $(55, 34, 9)$ feet in length, width and height respectively. The AP is mounted on one wall at location $\underline{r^s} : (24, 2, 6.5)$ and the receiver location $\underline{r^o}$ is varied. The vector orientation of the source and receiver is $\underline{u} = (1, 0, 0)$. The walls of the enclosure are assumed to have a constant relative dielectric contrast of $\epsilon = 3.0$. The sampling interval was chosen to be $T_s = 0.1$ ns. This broadband CIR was bandpass filtered to yield the CIR for a band centered at 2.4 Ghz and bandwidth of 40 Mhz. For the orientations considered, the E_1 component of the electric field is dominant and is considered to represent the channel impulse response (CIR).

The CIRs computed from the image model for the three spatial positions $A : (24, 15, 2.5), B : (3, 33, 2.5)$ and $C : (45, 14, 2.5)$ are depicted in Fig. 8. The top panel (a, b, c) includes the LOS component. In the bottom panel (d, e, f), the LOS signal was removed from the wideband CIR before bandpass filtering. For each location, the range on the vertical axis extends from the minimum to maximum range of $h[n]$ under LOS conditions. The horizontal axis n represents time sampled in intervals of 0.1 ns. The LOS for locations A, B, C occurs at $n = 138, 249, 382$ and the time to multipath is approximately $25, 14$ and 11 units from the direct signal. The figures clearly illustrate the room reverberation effect and its enhancement when the receiver is positioned at location C, a room corner. At such positions, the maximum number of characteristic modes of the enclosure are excited.

The multipath profile of the CIR can be distinguished into two regions, referred to as the coherent and diffuse regimes. The coherent regime is comprised of early arrivals from first and second order reflections. The diffuse regime corresponds to the tail of the CIR and consists of the incoherent response of a large number of higher order reflections. At locations A and B, the power in the coherent regime is small relative to the LOS signal and they are fairly separated in time and resolvable from the LOS. In contrast, at C, the strength of the early arrivals are comparable to the direct signal and appear in quick succession after the occurrence of the LOS signal. This is due to the close proximity to the two reflecting walls. These distinguishing features in the spatial variation of the CIR play an important role in influencing the performance of receivers that are designed to make use of multipath diversity. This aspect is examined in the next section.

4. PERFORMANCE OF CDMA IN MULTIPATH CHANNELS

The performance of a CDMA system under the influence of channel responses shown in Fig 8 will be examined in this section. A single user system is analyzed in keeping with the experimental setup. The data transmission rate is $R_b = \frac{1}{T}$ where T is the bit duration. The chip rate is $R_c = \frac{1}{T_c}$, where T_c is the chip duration which is set to 90.91 nsecs. The data signal $b(t) = \sum_{k=-\infty}^{\infty} b_k \; P_b(t - kT)$ where $b_k : \pm 1$ and $P_b(t)$ is a rectangular pulse of duration T and has unit energy. The spreading code signal is represented as $a(t) = \sum_{l=-\infty}^{\infty} a_k \; P_c(t - lT_c)$. The sequence $a_k : \pm 1, \; k = 1, ...N_c$ repeats at a period N_c and $P_c(t)$ is also a rectangular shaping pulse of duration T_c seconds. In the simulation the Barker sequence of length $N_c = 11$ is applied for spreading. Setting the bit duration $T = N_c T_c$, leads to a spreading gain of N_c. The baseband representation of the spread spectrum signal is,

$$v(t) = a(t)b(t) \tag{6}$$

This signal is BPSK modulated to yield the transmitted bandpass signal,

$$s(t) = Av(t) \; e^{j(\omega_c t + \theta)} \tag{7}$$

where ω_c and θ are the carrier frequency and phase respectively. The channel is represented by the real valued impulse response

$$h(t) = \sum_{m=0}^{M-1} \alpha_m \; \delta(t - \tau_m) \tag{8}$$

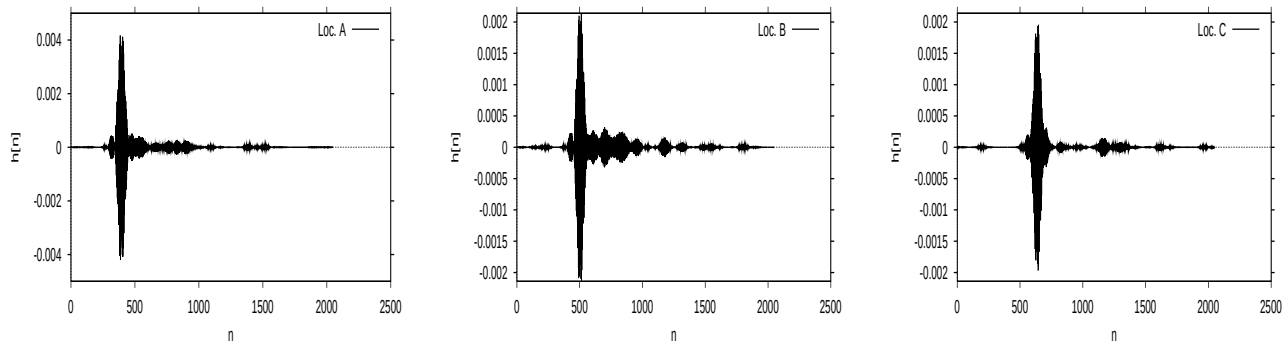

(a)Loc A: (b)Loc B (c) Loc C

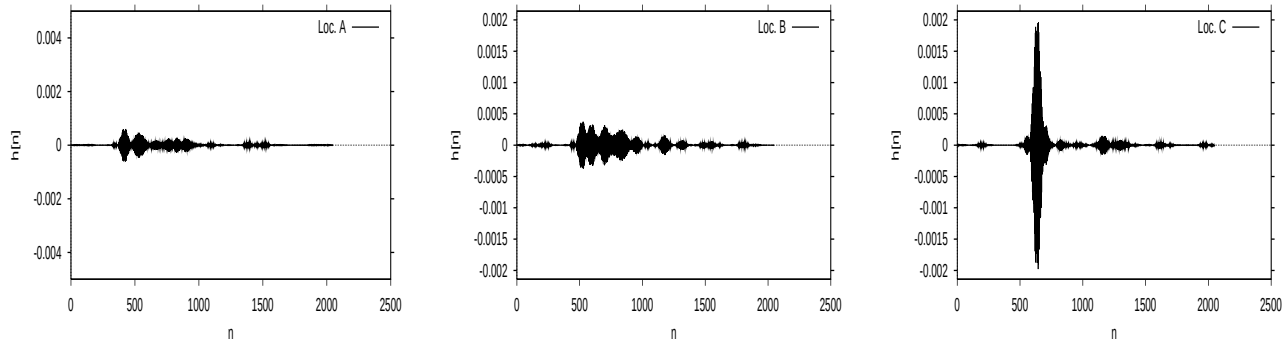

(d)Loc A (e)Loc B (f) Loc C

Figure 8. The channel impulse response for locations A, B, C with LOS and multipath (a,b,c) and with only multipath (d,e,f).

consisting of M resolvable paths with amplitudes α_m and path delays $\tau_m = mT_c$ sampled at the chip rate. The received signal is given as

$$r(t) = A \sum_{m=0}^{M-1} \alpha_m v(t - \tau_m) e^{j(\omega_c t + \gamma_m)} \tag{9}$$

where $\gamma_m = -\omega_c \tau_m$.

The additive interference is white Gaussian noise $n(t)$ with one-sided power spectral density N_0 W/hz. The receiver is the standard matched filter based correlator which is followed by demodulation and sampling. The filtered signal is represented as

$$z(t) = \int_0^T r(t)\ a(t)\ e^{-j\omega_c t} dt = A \sum_{m=0}^{M-1} \alpha_m\ v(t - \tau_m)\ e^{j\gamma_m}\ dt + \eta(t) \tag{10}$$

where $\eta(t)$ represents the filtered noise.

The receiver is assumed to be in perfect phase synchronization with the source. The case where the receiver recovers the signal from the LOS path is considered first. Referring to this path by the index $m = L$ and assuming $\gamma_M = 0$ and $\tau_M = 0$, the i^{th} symbol is detected based on the value,

$$z_i = A\alpha_L b_i R_a(0) + Ab_i \sum_{m \neq L} \alpha_m R_a(mT_c) + \eta_i \tag{11}$$

where $R_a(\tau)$ is the periodic autocorrelation function of $a(t)$. The second term in Eq. 11 represents the additional interference form multipath. The dominant multipath delays are assumed to be within one symbol interval.

Figs. 9 depicts the simulated bit error rate (BER) as a function of transmitted SNR for the receiver model described in Eq. 11. Here the receiver synchronizes to the LOS path and the performance is a function of the energy in the multipath signal. The BER for the ideal case of zero multipath energy is also shown for comparison. The multipath energy at A is higher contributing approximately $1-3$ dB loss to the signal power. In a real environment channel fading can limit the receiver from locking the LOS signal. In such a case, multipath power must be utilized for signal detection. In the second type of receiver considered, an L_r branch maximal

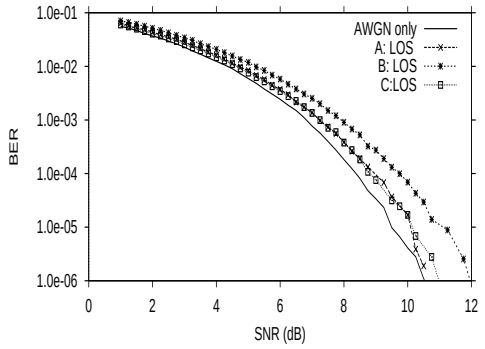

Figure 9. BER vs SNR with LOS detection in multipath.

ratio combining Rake receiver[7] was implemented using only the multipath signals. It is assumed that the CIR parameters are exactly known and the receiver is perfectly time and phase synchronized at every branch. The requirement on the size of L_r to achieve desired bit error rate performance is examined. This approach could be applied only to locations A and B where the multipath can be resolved in by sampling at the chip rate. At location C however, due to the rapid occurrence of early arrivals and small delay spread, channel sampling rate must be significantly increased for multipath combining to be effective. Fig. 10 shows the performance of the Rake receiver in NLOS detection at A and B. The required SNR must be increased by $3-4$ dB for A, whereas B requires an increase of $7-8$ dB signal power for performance comparable to LOS detection.

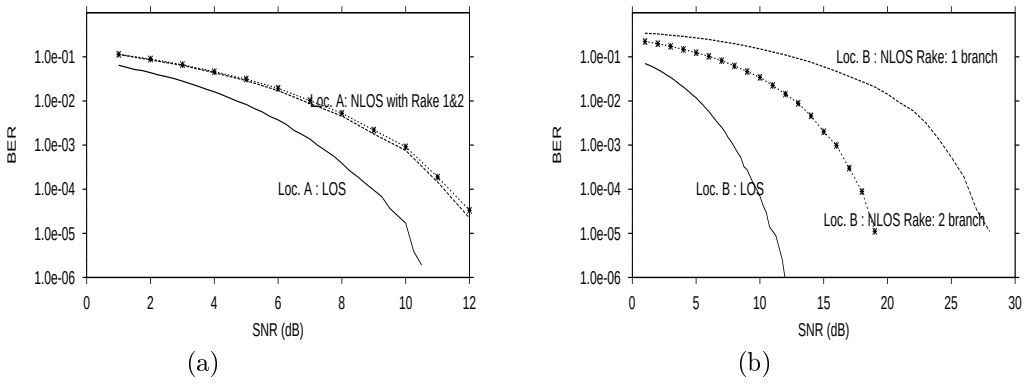

Figure 10. BER vs SNR with NLOS detection using a Rake receiver.

5. CONCLUSIONS

The performance of IEEE 802.11b wireless LAN products supporting 11 Mbps data rates in an indoor environment has been analyzed using TCP traffic, channel noise and signal power measurements. The average TCP throughput was found to be around 4.2 Mbps and generally independent of mobile receiver position with respect to the access point. The TCP packet retransmission rate and packet collision rate are however shown to increase in proportion to the multipath energy in the channel impulse response (CIR). An image-source based channel model is applied to estimate the CIR at the measurement locations. These CIR's are shown to provide quantitative evidence for the source of performance degradation at different positions in the room. The increase in multipath energy at particular locations in the channel, combined with small delay spread values are shown to limit the application of path diversity combining receivers.

ACKNOWLEDGMENTS

This work was supported in part by NSF grants ANI-9734585 and DUE-0123099

REFERENCES

1. I. S. 801-11, *IEEE Standard for Wireless LAN Medium Access Control (MAC) and Physical Layer (PHY) Specification*, 2001.
2. B. Crow, I. Widjaja, J. Kim, and P. Sakai, "Ieee 802.11 wireless local area networks," *IEEE Communication Magazine* , September 1997.
3. A. Kamerman and G. Aben, "Throughput performance of wireless lans operating at 2.4 and 5 ghz," in *11th IEEE International Symposium on Personal, Indoor and Mobile Radio Communications (PIMRC 2000)*, pp. 190–195, Sep. 2000.
4. G. Xylomenos and G. Polyzos, "Tcp and udp performance over a wireless lan," in *Proc. Infocom'99*, pp. 439–446, March 1999.
5. L. Munoz, M. Garcia, J. Choque, R. Aguero, and P. Mahonen, "Optimizing internet flows over ieee 802.11b wireless local area networks: A performance-enhancing proxy based on forward error correction," *IEEE Commun. Mag.* , pp. 60–67, December 2001.
6. M. C. A. DeSimone and O. Yue, "Throughput performance of transport-layer protocols over wireless lans," in *Proc. IEEE Globecom'93*, pp. 542–549, December 1993.
7. T. Rappaport, *Wireless Communications*, Prentice-Hall, 1996.
8. P. S. G.J.M. Janssen and R. Prasad, "Wideband indoor channel measurements and ber analysis of frequency selective multipath channels at 2.4, 4.75 and 11.5 ghz," *IEEE Trans. Comm.* , pp. 1272–1288, Oct. 1996.
9. H. Zepernick and T. Wysocki, "Multipath channell parameters for indoor radio at 2.4 ghz ism band," in *Proc. 49th IEEE Veh. Tech. Conf.*, pp. 190–193, 1999.
10. S. Kim, H. Bertoni, and M. Stern, "Pulse propagation characteristics at 2.4 ghz inside buildings," *IEEE Trans. Veh. Tech.* **45**, pp. 579–592, Aug. 1996.
11. G. Turin, "Introduction to spread-spectrum antimultipath techniques and their application to urban digital radio," *Proc. of the IEEE* **68**, pp. 328–352, March 1980.
12. B. N. G.T. Nguyen, R.H.Katz and M. Satyanarayanan, "A trace-based approach for modeling wireless channel behavior," in *Proc. Winter Simulation Conference*, pp. 597–604, Dec. 1996.
13. A. Sommerfeld, "Propagation of waves in wireless telegraphy," *Ann. Phys. (Paris)* **28**, pp. 665–736, 1909.
14. V. Lindell and E. Alanen, "Exact image theory for the sommerfeld half-space problem, part i: vertical magnetic dipole," *IEEE Trans. on Ant. and Prop.* **32**(2), pp. 126–133, 1984.
15. V. Lindell and E. Alanen, "Exact image theory for the sommerfeld half-space problem, part i: vertical electric dipole," *IEEE Trans. on Ant. and Prop.* **32**(8), pp. 841–847, 1984.
16. P. Sharma, P. Sachetta, C. Thompson, and K. Chandra, "Channel models for indoor wireless transmission," in *Proc. IEEE Intl. Conf. on 3G Wireless and Beyond*, pp. 48–53, May 2001.
17. J. Stratton, *Electromagnetic Theory*, McGraw-Hill, 1941.